

Resonant Damping of Kink Modes in Solar Coronal Slabs

Hui Yu · Bo Li · Shaoxia Chen ·
Mingzhe Guo

© Springer

Abstract We examine resonantly damped kink modes in straight coronal slabs, paying special attention to the effects of the formulation for the transverse density distribution (“profile” for brevity). We work in the framework of pressureless, gravity-free, resistive magnetohydrodynamics, and adopt the dissipative eigenmode perspective. The density profile is restricted to be one-dimensional, but nonetheless allowed to take a generic form characterized by a continuous transition layer connecting a uniform interior to a uniform exterior. A dispersion relation (DR) is derived in the thin-boundary limit, yielding analytical expressions for the eigenfrequencies that generalize known results in various aspects. We find that the analytical rather than the numerical solutions to the thin-boundary DR serve better the purpose for validating our self-consistent resistive solutions. More importantly, the eigenfrequencies are found to be sensitive to profile specifications, the ratio of the imaginary to the real part readily varying by a factor of two when one profile is used in place of another. Our eigenmode computations are also examined in the context of impulsively excited kink waves, suggesting the importance of resonant absorption for sufficiently oblique components when the spatial scale of the exciter is comparable to the slab half-width.

Keywords: Magnetohydrodynamics (MHD) – Coronal Seismology – Kink modes – Resonant absorption

1. Introduction

There has been ample observational evidence that the highly structured solar corona is replete with low-frequency waves and oscillations (see e.g., De Moortel

✉ B. Li
bbl@sdu.edu.cn

Shandong Provincial Key Laboratory of Optical Astronomy and Solar-Terrestrial Environment, Institute of Space Sciences, Shandong University, Weihai, 264209 Shandong, China

and Nakariakov 2012; Nakariakov *et al.* 2016; Nakariakov and Kolotkov 2020, for recent reviews). A customary practice, known as “coronal seismology” or more broadly “solar atmospheric seismology”, is then to place these observations in the theoretical framework of magnetohydrodynamic (MHD) waves in structured media, allowing one to infer the atmospheric parameters that prove difficult to directly measure (for topical issues, see e.g., Ballester *et al.* 2007, Nakariakov and Erdélyi 2009, Erdélyi and Goossens 2011, Van Doorselaere *et al.* 2020). From the theoretical perspective, wave-hosting structures have long been modeled as density-enhanced cylinders embedded in an otherwise uniform corona (e.g., Rosenberg 1970, Zajtsev and Stepanov 1975, Spruit 1982, Edwin and Roberts 1983, Cally 1986; see also the recent textbook by Roberts 2019). The subsequent applications to kink modes in active region (AR) loops, abundantly measured since the TRACE era (Aschwanden *et al.* 1999; Nakariakov *et al.* 1999), then enabled the inference of the magnetic field strength not only for individual loops (Nakariakov and Ofman 2001) but also over a substantial portion of an AR (Anfinogentov and Nakariakov 2019) or even across several ARs (Yang *et al.* 2020). While the axial phase speeds alone suffice for this purpose, the damping rates of coronal kink modes have also proved informative for inferring the information on the transverse density distribution (e.g., Aschwanden *et al.* 2003; Arregui *et al.* 2007b; Goossens *et al.* 2008; Arregui and Asensio Ramos 2014), provided that the damping can be accounted for by the resonant absorption in the Alfvén continuum (e.g., Ruderman and Roberts 2002; Goossens, Andries, and Aschwanden 2002). This information is known to be critical in wave-based mechanisms for coronal heating (e.g., Arregui 2015; Cranmer and Winebarger 2019) but difficult to glean even seismologically (e.g., Arregui 2018; Arregui and Goossens 2019).

There is a long history of theoretical examinations on MHD waves in magnetized slabs as well, in both non-solar (e.g., Tataronis and Grossmann 1973; Grossmann and Tataronis 1973; Hasegawa and Chen 1974; Chen and Hasegawa 1974) and solar contexts (e.g., Ionson 1978; Wentzel 1979a; Edwin and Roberts 1982). Focusing on the solar context, these examinations are important not only in their own right but prove necessary given the diversity of solar atmospheric structures (for recent studies, see e.g., Hornsey, Nakariakov, and Fludra 2014; Allcock and Erdélyi 2017; Oxley, Zsámberger, and Erdélyi 2020). Further restricting ourselves to coronal kink modes, we note that a slab configuration is indeed more relevant for interpreting such observations as sunward moving tadpoles in post-flare supra-arcades (Verwichte, Nakariakov, and Cooper 2005), oscillating AR arcades in response to flaring activities (Jain, Maurya, and Hindman 2015; Allian, Jain, and Hindman 2019), and large-scale propagating transverse motions of streamer stalks (“streamer waves”, Chen *et al.* 2010, 2011; Decraemer, Zhukov, and Van Doorselaere 2020). The application of a slab equilibrium to streamer waves seems somehow surprising given the current sheets embedded in streamer stalks, but is actually justifiable provided that current sheets can be regarded as infinitely thin and the electric resistivity can be neglected (e.g., Edwin, Roberts, and Hughes 1986; Feng *et al.* 2011).

This study is intended to examine resonantly damped coronal kink modes in pressure-less straight coronal slabs structured in a one-dimensional (1D) manner,

and can be regarded as an expansion of the study by Arregui *et al.* (2007a, A07 hereafter). For the ease of discussion, let the slab axis be directed in the z -direction. By “1D” we refer to a configuration where the equilibrium density is nonuniform only in the x -direction, but nonetheless takes a rather generic form comprising a transition layer (TL) that continuously connects a uniform interior to a uniform tenuous exterior. We further denote the axial and out-of-plane wavenumbers by k_z and k_y , respectively. For the configuration at hand, an extensive list of analytical studies has established that obliquely propagating ($k_y \neq 0$) kink modes are resonantly absorbed in the Alfvén continuum, provided that the TL width is finite ($l \neq 0$) (e.g., Ionson 1978; Wentzel 1979a; Hollweg and Yang 1988). To our knowledge, these studies tend to assume that $k_y \gg k_z$ and $k_y l \ll 1$, which were first lifted in the numerical study of A07. However, among the many observationally relevant parameters, only the influence of k_y was examined therein for a particular density profile specification (“profile” for brevity). Our study therefore differs from A07 in the following three ways. First, we will numerically explore a broader set of parameters for the same specification, and additionally examine two different profiles. The former aspect is necessary to address, given the evident influence of such additional parameters as the TL width on the damping rate. On the other hand, although exclusively pertaining to the case where $k_y = 0$, previous results have demonstrated the profile sensitivity of the dispersive properties of kink modes (e.g., Edwin and Roberts 1988; Lopin and Nagorny 2015; Yu *et al.* 2015; Chen *et al.* 2018b). Drawing analogy with pertinent cylindrical studies (Soler *et al.* 2013, 2014), one expects the same sensitivity for a non-vanishing k_y given that cylindrical results tend to be closely connected to slab ones when k_y is substantial (e.g., Goossens, Hollweg, and Sakurai 1992). Second, we will also provide analytical expressions for the eigenfrequencies in some limiting situations. While our approach is much-practiced, we will show that these expressions extend known solar results by allowing a broader range of k_y and non-solar results by allowing rather general profile choices. Third, we will connect our computations to impulsively generated kink waves, as likely to be relevant for, say, streamer waves. On this aspect we note that resonant absorption has been invoked to account for the rapid damping of the oscillatory motions of streamer stalks imaged with STEREO/COR1 (Kwon *et al.* 2013, Figure 6). It is just that the pertinent cylindrical theories were implicated therein, despite that a slab configuration seems more appropriate (e.g., Decraemer, Zhukov, and Van Doorselaere 2019).

This manuscript is organized as follows. Section 2 details the specification of our equilibrium configuration, and how we formulate and solve the pertinent eigenvalue problem. The numerical results are then presented in Section 3. Section 4 summarizes the present study, ending with some concluding remarks.

2. Model Description

2.1. Equilibrium Configuration

We adopt resistive, gravity-free MHD throughout, and additionally neglect the gas pressure. The primitive variables are then the mass density (ρ), velocity

(\mathbf{v}), and magnetic field (\mathbf{B}). We denote the equilibrium quantities with the subscript 0, and assume that no equilibrium flow is present ($\mathbf{v}_0 = 0$). Working in a Cartesian coordinate system (x, y, z), we take the equilibrium magnetic field to be uniform and directed in the z -direction ($\mathbf{B}_0 = B_0 \hat{z}$). We take the equilibrium density (ρ_0) to be structured only in the x -direction and symmetric about $x = 0$. The transverse profile for ρ_0 is further assumed to comprise a uniform interior with density ρ_i , a uniform exterior with density ρ_e , and a transition layer (TL) continuously connecting the two ($\rho_i > \rho_e$). The Alfvén speed is defined by $v_A^2 = B_0^2/(\mu_0 \rho_0)$, where μ_0 is the magnetic permeability in free space. We denote the values of v_A in the interior and exterior by v_{Ai} and v_{Ae} , respectively. To specify the density profile, it suffices to consider only the half-space $x \geq 0$,

$$\rho_0(x) = \begin{cases} \rho_i, & 0 \leq x < x_i = R - l/2, \\ \rho_{tr}(x), & x_i \leq x \leq x_e = R + l/2, \\ \rho_e, & x > x_e. \end{cases} \quad (1)$$

Evidently, this configuration mimics a density-enhanced slab of mean half-width R embedded in a uniform ambient. In addition, the TL width (l) lies in the range between 0 and $2R$. A number of much-employed TL profiles will be examined, namely (e.g., Ruderman and Roberts 2002; Soler *et al.* 2013; Yu *et al.* 2015)

$$\rho_{tr}(x) = \begin{cases} \frac{\rho_i}{2} \left[\left(1 + \frac{\rho_e}{\rho_i} \right) - \left(1 - \frac{\rho_e}{\rho_i} \right) \sin \frac{\pi(x-R)}{l} \right], & \text{sine}, \\ \rho_i - (\rho_i - \rho_e) \left(\frac{x-x_i}{l} \right), & \text{linear}, \\ \rho_i - (\rho_i - \rho_e) \left(\frac{x-x_i}{l} \right)^2, & \text{parabolic}. \end{cases} \quad (2)$$

We note that A07 was dedicated to a “sine” profile. Figure 1 illustrates both our equilibrium configuration and the density profiles. For illustration purposes, the density contrast (ρ_i/ρ_e) and the dimensionless TL width (l/R) are chosen to be 10 and 0.75, respectively.

2.2. Formulation of the Eigenvalue Problem and Method of Solution

Let the subscript 1 denote small-amplitude perturbations to the equilibrium. The linearized resistive MHD equations then read

$$\rho_0 \frac{\partial \mathbf{v}_1}{\partial t} = \frac{(\nabla \times \mathbf{B}_1) \times \mathbf{B}_0}{\mu_0}, \quad (3)$$

$$\frac{\partial \mathbf{B}_1}{\partial t} = \nabla \times \left(\mathbf{v}_1 \times \mathbf{B}_0 - \frac{\eta}{\mu_0} \nabla \times \mathbf{B}_1 \right). \quad (4)$$

Here η is the Ohmic resistivity, taken to be constant for simplicity. We adopt an eigenvalue-problem (EVP) standpoint by Fourier-analyzing any perturbation as

$$f_1(x, y, z; t) = \text{Re}\{\tilde{f}(x) \exp[-i(\omega t - k_y y - k_z z)]\}, \quad (5)$$

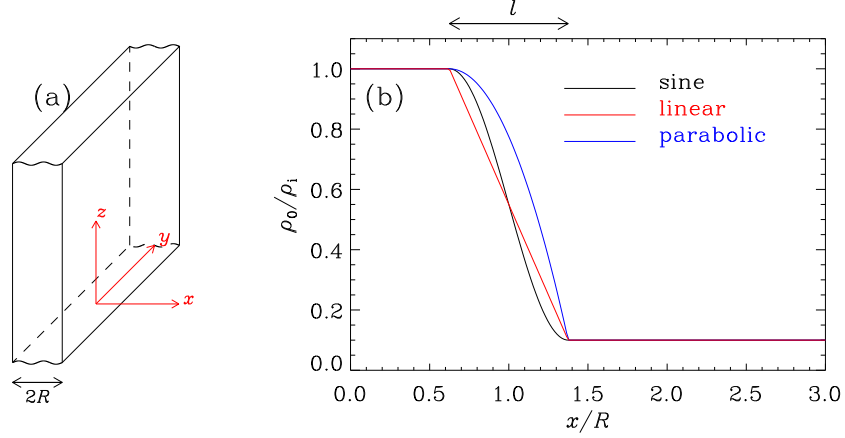


Figure 1. (a) Schematic illustration of the equilibrium configuration, and (b) transverse distributions of the equilibrium density ρ_0 . All density profiles are characterized by a transition layer (TL) that continuously connects a uniform interior to a uniform exterior. This TL is located between $x_i = R - l/2$ and $x_e = R + l/2$, where R is the mean slab half-width and l the TL width. For illustration purposes, the density contrast (ρ_i/ρ_e) and the dimensionless TL width (l/R) are chosen to be 10 and 0.75, respectively.

where ω is the angular frequency, and k_z (k_y) represents the axial (out-of-plane) wavenumber. With tilde we denote the Fourier amplitude. We take k_y and k_z as real-valued, but allow ω to be complex-valued. If some quantity is complex, then we denote its real and imaginary parts with subscripts R and I, respectively. Note that $\omega_I < 0$ throughout. In component form, Equations (3) and (4) become

$$\omega \tilde{v}_x = -\frac{B_0}{\mu_0 \rho_0} \left(k_z \tilde{B}_x + i \tilde{B}_z' \right), \quad (6)$$

$$\omega \tilde{v}_y = -\frac{B_0}{\mu_0 \rho_0} \left(k_z \tilde{B}_y - k_y \tilde{B}_z \right), \quad (7)$$

$$\omega \tilde{B}_x = -B_0 k_z \tilde{v}_x + \frac{i\eta}{\mu_0} \left[\tilde{B}_x'' - (k_y^2 + k_z^2) \tilde{B}_x \right], \quad (8)$$

$$\omega \tilde{B}_y = -B_0 k_z \tilde{v}_y + \frac{i\eta}{\mu_0} \left[\tilde{B}_y'' - (k_y^2 + k_z^2) \tilde{B}_y \right], \quad (9)$$

$$\omega \tilde{B}_z = -iB_0 (\tilde{v}_x' + i k_y \tilde{v}_y) + \frac{i\eta}{\mu_0} \left[\tilde{B}_z'' - (k_y^2 + k_z^2) \tilde{B}_z \right], \quad (10)$$

where we have used the shorthand notation $' \equiv d/dx$. Equations (6) to (10) constitute a standard EVP when supplemented with appropriate boundary conditions (BCs). With kink modes in mind, we specify the BCs at the slab axis ($x = 0$) as $\tilde{v}_x' = \tilde{v}_y = \tilde{B}_x' = \tilde{B}_y = \tilde{B}_z = 0$. Only trapped modes are of interest, in accordance with which all variables are required to vanish when $x \rightarrow \infty$.

The solution procedure for the EVP is as follows. We start with normalizing Equations (6) to (10), for which purpose we take R , v_{Ai} , and ρ_i as the independent normalizing constants. The derivative normalizing constants for time and magnetic field are chosen to be R/v_{Ai} , and $B_i \equiv \sqrt{\mu_0 \rho_i v_{Ai}^2}$, respectively. The Ohmic resistivity is wrapped up in the magnetic Reynolds number

$R_m = \mu_0 R v_{Ai} / \eta$. We formulate and solve the EVP with the general-purpose finite-element code PDE2D (Sewell 1988), which was first introduced into the solar context by Terradas, Oliver, and Ballester (2006) to our knowledge. We adopt a computational domain of $[0, x_M]$, and place the outer boundary (x_M) sufficiently far from the slab such that further increasing x_M does not influence our numerical results. A nonuniform grid is employed to save computational cost, and a considerable fraction of the grid points is deployed in the TL to resolve the possible oscillatory behavior therein. It turns out that the details of the grid setup have some bearings on the parameter range that we can explore. To illustrate this, we recall that the resistive approach here is not intended to explore the full spectrum of resistive eigenmodes. Rather, we are interested only in the one that falls back to the standard kink mode when the TL is infinitely thin ($l = 0$) and the resistivity vanishes ($\eta = 0$). Allowing l to be finite, we are adopting the well known resistive eigenmode approach to examine the essentially ideal process of the resonant absorption of a collective mode in the relevant continuum (e.g., Poedts and Kerner 1991; Van Doorselaere *et al.* 2004; Terradas, Oliver, and Ballester 2006; Guo *et al.* 2016; Chen *et al.* 2018a) or continua (e.g., Soler *et al.* 2009; Chen *et al.* 2020). As such, we are looking for only those eigenfrequencies that do not depend on R_m when R_m is sufficiently large. This is illustrated by Figure 2 where the ratio of the imaginary to the real part of the eigenfrequency (or $-\omega_I/\omega_R$ to be precise) is shown as a function of the magnetic Reynolds number (R_m) for a “sine” density profile with $\rho_i/\rho_e = 10$. In addition, $[k_y R, k_z R]$ is fixed at $[1, \pi/50]$. A series of l/R , equally spaced by 0.01, is examined except for the lowermost curve. The outer boundary is fixed at $x_M = 50 R$. Furthermore, 18000 uniformly spaced grid points are employed for $x \leq 3 R$, beyond which the grid spacing increases by a constant factor of 1.00125. For a given l/R , one sees that the eigenfrequencies are indeed R_m -independent over an interval of R_m , for which the left and right ends are to be denoted by $R_{m,L}$ and $R_{m,R}$, respectively. Evidently, the sought-after eigenfrequencies can be confidently identified only when the interval $[R_{m,L}, R_{m,R}]$ is sufficiently broad. However, this cannot be guaranteed. On the one hand, $R_{m,L}$ tends to increase with l/R . On the other hand, our code does not converge when R_m becomes too large for the well known reason that the eigenfunctions become increasingly oscillatory in the so-named dissipative layers (DLs) (see e.g., Figure 4 in Ruderman, Tirry, and Goossens 1995 and Figure 1 in Tirry and Goossens 1996). On top of that, Figure 2 indicates that some zigzags appear when R_m approaches the maximal value that the code can handle, the end result being that the interval $[R_{m,L}, R_{m,R}]$ narrows with l/R . Numerically speaking, this interval can be made broader by employing more grid points to resolve the fine scales in the DLs. However, this mitigation comes at the price that the computational resources will become increasingly demanding. Overall, we find that this numerical difficulty arises when the damping is too heavy, which occurs when l/R and/or $k_y R$ are too large.

This technical issue notwithstanding, it proves possible to expand the parameter range examined by A07 where the “sine” profile is adopted. In addition, it is possible to examine another two profiles as stated in Equation (2). For the

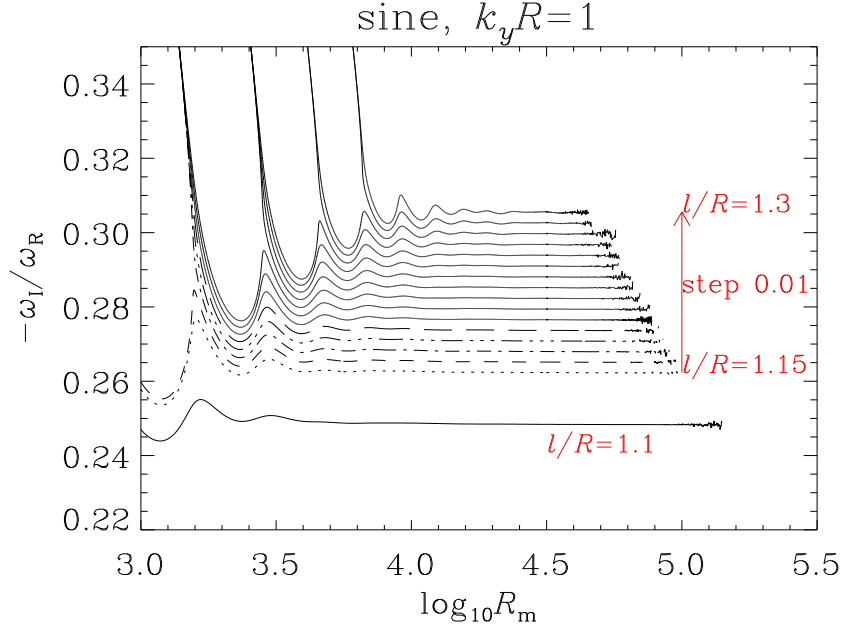


Figure 2. Dependence on the magnetic Reynolds number (R_m) of the ratio of the imaginary to the real part of the eigenfrequency ($-\omega_I/\omega_R$) of resonantly damped kink modes in coronal slabs. A “sine” profile is adopted for the equilibrium density, and the density contrast ρ_i/ρ_e is chosen to be 10. A number of values are examined for the dimensionless transition layer width (l/R), with l/R evenly spaced by 0.01 with the exception of the curve labeled $l/R = 1.1$. The axial and out-of-plane wavenumbers correspond to $k_z R = \pi/50$ and $k_y R = 1$, respectively.

ease of description, we formally express the eigenfrequencies as

$$\frac{\omega R}{v_{Ai}} = \mathcal{G} \left(\text{prof}, \frac{\rho_i}{\rho_e}, \frac{l}{R}; k_y R, k_z R \right), \quad (11)$$

where “prof” represents a prescription for the equilibrium density profile. The magnetic Reynolds number does not appear in Equation (11), which means in practice that the computed eigenfrequencies are found in an interval of $[R_{m,L}, R_{m,R}]$ spanning at least half a decade or so.

2.3. Resonantly Damped Kink Modes in the Thin-Boundary Limit

The functional dependence in Equation (11) can be established analytically in a number of situations. This subsection is intended to expand some available results, for which purpose we start by noting that the ideal version ($\eta = 0$) of Equations (6) to (10) can be manipulated to yield a single equation governing \tilde{v}_x (e.g., A07), namely

$$\left[\frac{k_z^2 - \omega^2/v_A^2}{k_y^2 + k_z^2 - \omega^2/v_A^2} \tilde{v}_x' \right]' - (k_z^2 - \omega^2/v_A^2) \tilde{v}_x = 0. \quad (12)$$

Evidently, the Alfvén resonance takes place at $x = x_A$ where $\omega_R = k_z v_A$. We now distinguish between two schools of approaches for treating resonantly damped modes. In one school, broadly referred to as the ideal quasi-mode approach, dissipative effects are mathematically irrelevant and a non-vanishing ω_I is accounted for by, say, analytically continuing the Green function (for early studies in various contexts, see e.g., Tataronis and Grossmann 1973, Grossmann and Tataronis 1973, Hasegawa and Chen 1974, Chen and Hasegawa 1974, Ionson 1978, Wentzel 1979b; see also the review by Goossens, Erdélyi, and Ruderman 2011). Equation (12) is involved in a substantial number of quasi-mode studies, which tend to assume $k_y^2 \gg k_z^2$ and $k_y^2 \gg |k_z^2 - \omega^2/v_A^2|$ from the outset, and address a “linear” density profile. Of particular relevance is the one in the fusion context by Tatsuno and Wakatani (1998, hereafter TW98; see also references therein), who showed that adopting a linear profile enables one to derive an analytical dispersion relation (DR) valid for arbitrary TL widths. As a result, the resonant damping is allowed to be heavy. Another school, referred to as the dissipative eigenmode approach and hence involving dissipative factors by construction, does not restrict the range of k_y but nonetheless assumes weak damping by working in the so-called thin-boundary (TB) limit ($l/R \ll 1$). However, no restriction is necessary for the equilibrium profile (e.g., Sakurai, Goossens, and Hollweg 1991; Goossens, Hollweg, and Sakurai 1992; Ruderman, Tirry, and Goossens 1995, to name only a few). We will follow the second approach.

We proceed by defining

$$\kappa_{i,e}^2 = k_z^2 - \frac{\omega^2}{v_{Ai,e}^2}, \quad (13)$$

$$m_{i,e}^2 = k_y^2 + k_z^2 - \frac{\omega^2}{v_{Ai,e}^2}, \quad (14)$$

where $-\pi/2 < \arg \kappa_{i,e}, \arg m_{i,e} \leq \pi/2$. Trapped kink modes then correspond to the following solution to Equation (12) in the uniform portions

$$\tilde{v}_x(x) = \begin{cases} A_1 \cosh(m_i x), & 0 < x < x_i, \\ A_2 \exp(-m_e x), & x > x_e, \end{cases} \quad (15)$$

where A_1 and A_2 are constants. In addition, the Fourier amplitude of the Eulerian perturbation of total pressure ($p_{\text{tot}} = \mathbf{B}_0 \cdot \mathbf{B}_1/\mu_0 = B_0 B_{1z}/\mu_0$) reads

$$\tilde{p}_{\text{tot}}(x) = \begin{cases} \left(\frac{B_0^2}{\mu_0}\right) \left(\frac{-iA_1}{\omega}\right) \left(\frac{\kappa_i^2}{m_i}\right) \sinh(m_i x), & 0 < x < x_i, \\ \left(\frac{B_0^2}{\mu_0}\right) \left(\frac{iA_2}{\omega}\right) \left(\frac{\kappa_e^2}{m_e}\right) \exp(-m_e x), & x > x_e. \end{cases} \quad (16)$$

Let $[q]$ denote the variation of some perturbation q across some thin dissipative layer bracketing the resonance. Furthermore, let $\tilde{\xi}_x$ denote the Fourier amplitude of the x -component of the Lagrangian displacement ($\tilde{v}_x = -i\omega\tilde{\xi}_x$). Assuming $l/R \ll 1$, the TB approximation attributes the variation of q across the TL to

$[q]$, and $[\tilde{p}_{\text{tot}}]$ and $[\tilde{\xi}_x]$ were found to be (e.g., Tirry and Goossens 1996; Andries, Tirry, and Goossens 2000)

$$[\tilde{p}_{\text{tot}}] = 0, \quad (17)$$

$$[\tilde{\xi}_x] = -\frac{i\pi k_y^2 \text{sgn}(\omega_R)}{\rho_A |\Delta_A|} \tilde{p}_{\text{tot},A}, \quad (18)$$

where any quantity designated with a subscript A is evaluated at the Alfvén resonance. Equations (17) and (18) are a slab generalization of the cylindrical version established by Sakurai, Goossens, and Hollweg (1991). The symbol Δ_A was also introduced therein, and reads for the present slab configuration

$$\Delta_A = \frac{d(\omega^2 - k_z^2 v_A^2)}{dx} \Big|_{x=x_A}. \quad (19)$$

With the jump conditions (17) and (18), one can connect \tilde{v}_x and \tilde{p}_{tot} in the interior and exterior, thereby establishing the following DR

$$\coth(m_i R) = -\left(\frac{\kappa_i^2}{\kappa_e^2}\right) \left(\frac{m_e}{m_i}\right) + i\pi \left(\frac{k_y^2}{k_z^2}\right) \left(\frac{\rho_A}{\rho'_A}\right) \left(\frac{\kappa_i^2}{m_i}\right). \quad (20)$$

Here ω_R is taken to be positive without loss of generality. We have also used the fact that $v_A^2(x) \propto 1/\rho(x)$ and $\rho' < 0$ in our equilibrium setup.

Equation (20) is analytically tractable when one assumes that $k_y^2 \gg |\omega^2/v_A^2|$, in which case $m_i \approx m_e \approx k_y$. Further assuming that $k_y l \ll 1$ and $|\omega_I| \ll \omega_R$, one proceeds by keeping only the terms linear in ω_I . The real part of the right-hand side (RHS) of Equation (20) is dominated by the first term, resulting in ¹

$$\omega_R^2 = k_z^2 v_{Ai}^2 \frac{1 + \Theta}{\rho_e/\rho_i + \Theta}, \quad (21)$$

where $\Theta = \tanh(k_y R)$. With the aid of Equation (21), the leading terms of the imaginary part of Equation (20) lead to that

$$\frac{\omega_I}{\omega_R} = -\frac{\pi}{2} \left(k_y \left|\frac{\rho_A}{\rho'_A}\right|\right) \frac{(1 - \rho_e/\rho_i)^2 \Theta^2}{(\rho_e/\rho_i + \Theta)^2 (1 + \Theta)}. \quad (22)$$

¹Neglecting the second term at this step leads to Equation (21) and then to Equation (22), with which one can come back to evaluate the real part of the second term. To maintain consistency, this real part should be far smaller than the LHS, which evaluates to $1/\Theta$. The end result is that the following inequality should be valid,

$$\left[\pi k_y \left(\frac{\rho_A}{\rho'_A}\right)\right]^2 \frac{(1 - \rho_e/\rho_i)^2 \Theta^3}{(\rho_e/\rho_i + \Theta)^3} \ll 1.$$

Specializing to the profiles considered in this study, one finds with Equation (24) that

$$(k_y l)^2 (\pi g)^2 \frac{\Theta^3}{(1 + \Theta)^2 (\rho_e/\rho_i + \Theta)} \ll 1.$$

By requiring $k_y l \ll 1$ we actually mean the situations where the afore-mentioned inequalities hold, which may be less restrictive.

As intuitively expected, ω_R as given by Equation (21) does not involve the specific prescription for the density profile. Consequently, the density at the resonance always evaluates to $\rho_A = (\rho_e + \Theta\rho_i)/(1 + \Theta)$. However, the profile specification does influence ω_I through the ρ'_A term in Equation (22). To evaluate this term, it can be readily found that the resonance takes place at

$$\frac{x_A - R}{l} = \begin{cases} \frac{1}{\pi} \arcsin\left(\frac{1 - \Theta}{1 + \Theta}\right), & \text{sine,} \\ \frac{1}{1 + \Theta} - \frac{1}{2}, & \text{linear,} \\ \left(\frac{1}{1 + \Theta}\right)^{1/2} - \frac{1}{2}, & \text{parabolic.} \end{cases} \quad (23)$$

It then follows that

$$\rho'_A = -\left(\frac{\rho_i - \rho_e}{l}\right) \frac{1}{g}, \quad (24)$$

where

$$g = \begin{cases} \frac{1 + \Theta}{\pi\sqrt{\Theta}}, & \text{sine,} \\ 1, & \text{linear,} \\ \left(\frac{1 + \Theta}{4}\right)^{1/2}, & \text{parabolic.} \end{cases} \quad (25)$$

Eventually, the TB damping rate can be expressed as

$$\frac{\omega_I}{\omega_R} = -\frac{\pi}{2} (k_y l) g \frac{(1 - \rho_e/\rho_i)\Theta^2}{(\rho_e/\rho_i + \Theta)(1 + \Theta)^2}. \quad (26)$$

We now compare our TB expressions with some previous results. We start by considering a further limit where $k_y R$ is large enough to ensure $\Theta \approx 1$. In this case, Equation (21) simplifies to

$$\omega_R^2 = \omega_k^2 \equiv k_z^2 c_k^2, \quad (27)$$

where

$$c_k^2 = \frac{2v_{Ai}^2}{1 + \rho_e/\rho_i} \quad (28)$$

defines the kink speed. Likewise, Equation (26) yields that

$$\frac{\omega_I}{\omega_R} = -\frac{\pi}{8} (k_y l) g \frac{\rho_i - \rho_e}{\rho_i + \rho_e}. \quad (29)$$

To proceed, we note that g now evaluates to $2/\pi$, 1, and $1/\sqrt{2}$ for the sine, linear, and parabolic profiles, respectively. Consider the linear profile for now. Equation (29) recovers the cylindrical result obtained by Goossens, Hollweg,

and Sakurai (1992, Equation (79b)), who were the first to adopt the jump conditions to examine quasi-modes from the dissipative eigenmode perspective to our knowledge. As suggested therein, the comparison between the slab and cylindrical configurations is possible by interpreting R as the cylinder radius and prescribing k_y with $1/R$. Indeed, adopting this prescription in Equation (29) further recovers the cylindrical results for the sine (Ruderman and Roberts 2002, Equation (72)) and parabolic profiles (Soler *et al.* 2014, Equation (7)). Now focus on the slab configuration. For a linear profile, Equations (27) and (29) have been obtained in an extensive list of studies using the ideal quasi-mode approach (e.g., Ionson 1978; Wentzel 1979a, to name only a few early studies). Among the quasi-mode studies, to our knowledge, TW98 were the only one that offered explicit expressions for the eigenfrequencies without requiring $\Theta \approx 1$. It is reassuring to see that Equation (15) therein is exactly reproduced by our Equations (21) and (26), which are derived with the dissipative eigenmode approach². Our Equation (22) therefore generalizes the TW98 results by allowing the TL profile to be as arbitrary as the TB approach allows. Likewise, it generalizes those dissipative eigenmode results where $\Theta \approx 1$ is assumed (Equation (57) in Ruderman, Tirry, and Goossens 1995, see also the references therein, in particular Mok and Einaudi 1985, and Hollweg and Yang 1988).

To sum up at this point, the DR (20) applies to rather arbitrary density profiles, provided $l/R \ll 1$. Furthermore, it is valid for arbitrary values of k_y and k_z . When $k_y^2 \gg |\omega^2/v_A^2|$ and $k_y l \ll 1$, the real part of the eigenfrequency is expressible by Equation (21). Likewise, the imaginary part is given by Equation (22) for general profiles, and specializes to Equation (26) for our profile choices. However, in the more general situation, Equation (20) needs to be solved numerically after one specifies the parameters in the parantheses in Equation (11). We adopt an iterative approach for this purpose, starting with an initial guess for ω_R such that a temporary value for x_A can be found. We then evaluate the ρ_A/ρ'_A term and solve Equation (20) to yield ω . Adopting this updated ω as a further guess, we iterate this process until it converges to a unique eigenfrequency.

3. Numerical Results

We are now in a position to examine the dispersive properties of resonantly damped kink modes in coronal slabs, for which purpose it is admittedly difficult to exhaust the full parameter space as contained in Equation (11). We choose to fix the density contrast at $\rho_i/\rho_e = 10$ throughout, a value representative of both active region loops (e.g., Aschwanden, Nakariakov, and Melnikov 2004) and streamer stalks (e.g., Chen *et al.* 2011, Figure 2). Our examination then starts with Figure 3, where the dependencies on the dimensionless TL width (l/R)

²Neglecting the gas pressure, one readily finds that Equation (15a) in TW98 is identical to Equation (21) here. However, our Equation (26) with $g = 1$ seems different from Equation (15b) in TW98. This discrepancy is only apparent, and can be readily reconciled by noting that $\Theta/(1 + \Theta) = [1 - \exp(-2k_y R)]/2$.

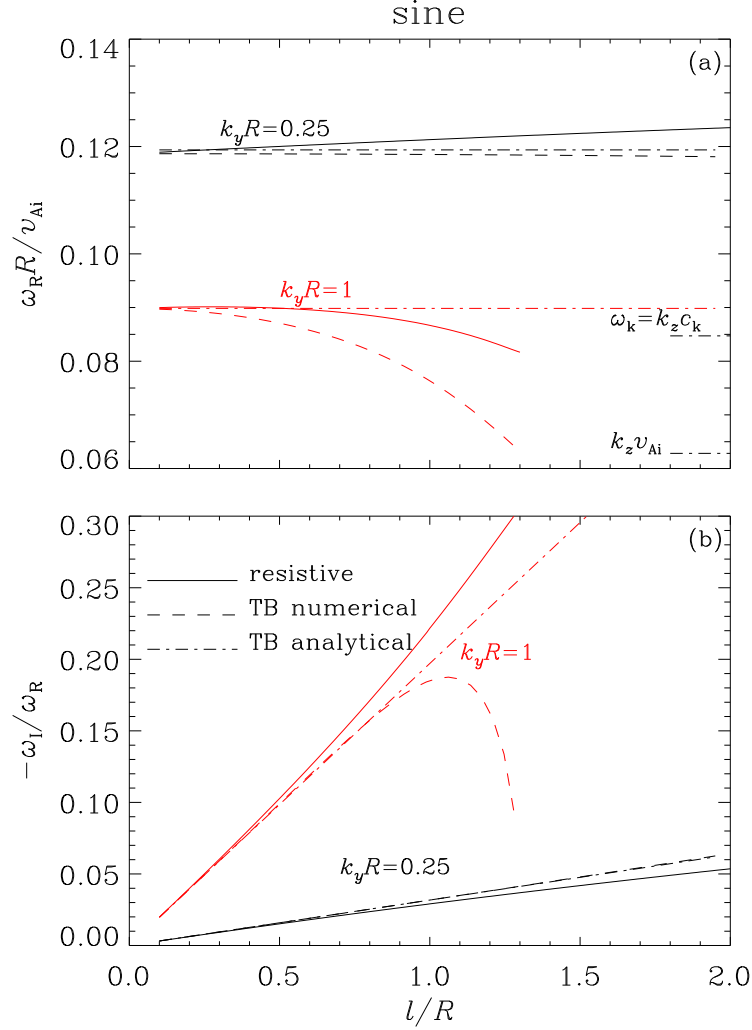


Figure 3. Dispersive properties of resonantly damped kink modes in coronal slabs. Shown here are the dependencies on the dimensionless TL width (l/R) of (a) the real part of the eigenfrequency (ω_R), and (b) the ratio of the imaginary to the real part ($-\omega_I/\omega_R$). The solid lines represent the results obtained with resistive computations, while the dashed ones correspond to the numerical solutions to the explicit DR (20) valid in the thin-boundary (TB) limit ($l/R \ll 1$). The analytical solutions to this DR, nominally valid when $k_y^2 \gg |\omega^2/v_A^2|$ and $k_y l \ll 1$, are plotted by the dash-dotted curves (see Equations (21) and (26) for details). Two different values of k_y are examined as labeled. For comparison, the horizontal bars represent the angular frequencies $k_z v_{Ai}$ and $\omega_k = k_z c_k$. A “sine” profile is adopted for the equilibrium density, the density contrast is fixed at $\rho_i/\rho_e = 10$, and the axial wavenumber is fixed at $k_z R = \pi/50$.

are shown for both the real part of the eigenfrequency (ω_R , Figure 3a), and the ratio of the imaginary to the real part ($-\omega_I/\omega_R$, Figure 3b). The equilibrium density profile is chosen to be a “sine” one for illustration purposes, and the axial wavenumber is fixed at $k_z R = \pi/50$. Two rather different values of k_y are examined as represented by the curves in different colors. The results from the self-consistent resistive computations are shown by the solid lines. We also solve the explicit DR (20) in the thin-boundary (TB) limit with both the iterative and analytical approaches, and label the corresponding results with “TB numerical” (the dashed curves) and “TB analytical” (dash-dotted), respectively. Two additional frequencies, $k_z v_{Ai}$ and $\omega_k = k_z c_k$, are also plotted for comparison (see the horizontal ticks in Figure 3a). Examining the TB curves, one sees that the “TB analytical” ones as given by Equations (21) and (26) tend to satisfactorily reproduce the “TB numerical” solutions when $k_y l$ is small, which is evidenced by the close agreement between the black dashed and dash-dotted curves pertaining to $k_y R = 0.25$. This is expected given that $k_y l \ll 1$ is assumed for deriving these expressions and that the additional assumption $k_y^2 \gg |\omega^2/v_A^2|$ tends to hold here. From Figure 3a one also sees that the dash-dotted curves may differ substantially from the kink frequency ω_k when $k_y R$ is not sufficiently large, suggesting the need to incorporate the k_y -dependence in analytical expressions for the eigenfrequency. These details aside, it is more important to note that, relative to the “TB analytical” curves, the “TB numerical” ones tend to deviate more significantly from the resistive results. This happens despite that the iterative solution to DR (20) seems more self-consistent than its analytical counterpart. On top of that, the iterative approach does not converge when $l/R \gtrsim 1.3$ for $k_y R = 1$, the reason being that ω_R decreases towards $k_z v_{Ai}$ as l/R increases and eventually leaves the Alfvén continuum. While only a “sine” profile is shown, we find that the resistive results tend to agree better with the “TB analytical” rather than the “TB numerical” results for other profile prescriptions as well. From this we conclude that, technically speaking, if one would like to invoke the TB limit to validate the eigenfrequencies numerically found for resonantly damped kink modes in coronal slabs with an equilibrium configuration similar to ours, then it is not worthwhile to further solve the relevant DR numerically. Analytical expressions similar to Equations (21) and (22) serve this purpose better.

Having validated our numerical approach, we will present only the resistive results from here onward. Before proceeding, however, we note that the red solid curves in Figure 3 do not extend to $l/R \gtrsim 1.3$. This is due to numerical rather than physical reasons. As has been discussed in connection to Figure 2, our resistive code has convergence difficulties when resonant damping is too heavy, which in general happens when $k_y l$ is large. This issue turns out to be even more prominent for the linear profile, as can be seen in Figure 4 where the l/R -dependencies of ω_R (the upper row) and $-\omega_I/\omega_R$ (lower) are compared between the sine and linear (parabolic) profiles in the left (right) column. Different colors are adopted to differentiate different profiles. Likewise, different linestyles pertain to a number of different values for k_y . The combination $[\rho_i/\rho_e, k_z R]$ is fixed at $[10, \pi/50]$. One sees that when $k_y R = 1$, our parabolic (the blue dash-dotted curves) and linear (red) computations manage to reach only $l/R \approx 1$ and 0.55 ,

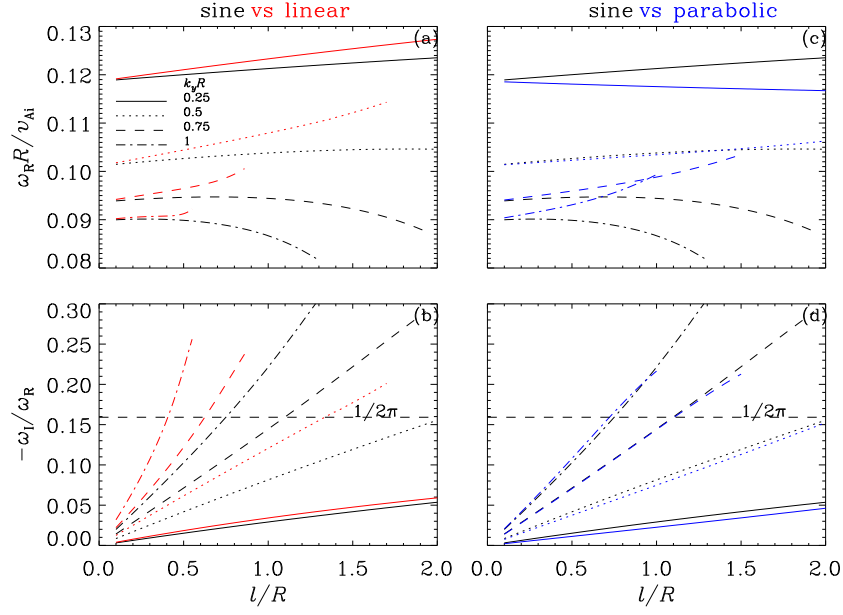


Figure 4. Influence of the density profile prescription on the dispersive properties of resonantly damped kink modes in coronal slabs. Shown here are the dependencies on the dimensionless TL width (l/R) of both the real part of the eigenfrequency (ω_R , the top row) and the ratio of the imaginary to the real part ($-\omega_I/\omega_R$, lower). Different profiles are differentiated by different colors, and a number of k_y are examined as represented by different linestyles. The horizontal dashed line in the lower row corresponds to $1/2\pi$, at which value the damping-time-to-period ratio attains unity. The pair of $[\rho_i/\rho_e, k_z R]$ is fixed at $[10, \pi/50]$.

respectively. Despite this, however, it is already evident that the profile prescriptions are important for determining the eigenfrequencies in general and the damping rates in particular. Take $l/R = 0.55$ for instance. Figure 4b indicates that $-\omega_I/\omega_R$ for the linear profile attains ~ 0.26 , a value considerably larger than its sine counterpart (~ 0.11). On the other hand, from Figure 4a one sees that the real parts of the eigenfrequencies for the two profiles do not differ much, meaning that the significant differences in $-\omega_I/\omega_R$ essentially derive from the differences in ω_I . Now consider the comparison between the sine and parabolic results as given in the right column. One can discern some profile dependence of ω_R in Figure 4c, but can hardly tell the two density profiles apart by inspecting $-\omega_I/\omega_R$ in Figure 4d. Overall, the point to draw from Figure 4 is that the effect of density profile specifications is quite subtle, by which we mean that in general one cannot tell beforehand whether ω_R or $-\omega_I/\omega_R$ experiences a larger variation when one switches from one profile to another.

The profile dependence can be brought out from another perspective, for which purpose we note that the horizontal dashed lines in the lower row in Figure 4 represent $1/2\pi$. Evidently, this corresponds to the situation where the ratio of the damping time to period attains unity, which may serve as a dividing line separating the under-damped from over-damped modes. For each profile, we can therefore deduce a critical TL width $(l/R)_{\text{crit}}$ at a given k_y . Surveying a more extensive range of k_y then leads to Figure 5, where $(l/R)_{\text{crit}}$ is plotted as

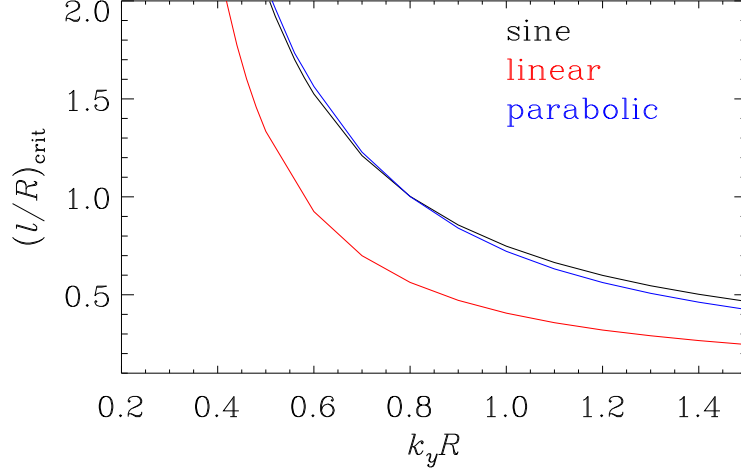


Figure 5. Influence of the density profile prescription on the dispersive properties of resonantly damped kink modes in coronal slabs. Shown here is the dependence on k_y of the critical dimensionless TL width $(l/R)_{\text{crit}}$, at which value $|\omega_I/\omega_R|$ attains $1/2\pi$. Different colors are adopted to represent different density profiles. The pair of $[\rho_i/\rho_e, k_z R]$ is fixed at $[10, \pi/50]$.

a function of k_y in different colors for different profile choices. One sees that the curves labeled “sine” and “parabolic” are close to one another, understandable given the insignificant differences in $-\omega_I/\omega_R$ between the two profiles. However, these two curves deviate considerably from the curve labeled “linear”, which is true throughout the entire range of k_y examined here.

The computations so far correspond to a fixed axial wavenumber of $k_z R = \pi/50$, which is more relevant for standing kink modes trapped in, say, AR loops or AR arcades. However, examining other values of k_z will be informative to say the least, and we look back at the parameters in the parentheses in Equation (11) for this purpose. If we allow only k_y to vary and construct a plot similar to Figure 4b, then we end up with a critical $k_{y,\text{crit}}$ that corresponds to $-\omega_I/\omega_R = 1/2\pi$. Further varying k_z therefore leads to a series of $k_{y,\text{crit}}$, and the output from such a practice with $l/R = 0.5$ is plotted in Figure 6. Here different density profiles are represented by the solid curves in different colors. When placed in the $k_y - k_z$ plane, the under-damped (over-damped) modes then lie below (above) the relevant solid curve for a specific profile prescription. Above all, one sees once again the importance of profile prescriptions for determining the dispersive properties of resonantly damped modes. When examined this way, not only does the curve labeled “linear” lie at quite some distance away from the rest, but also some substantial difference arises between the curves labeled “sine” and “parabolic”.

Figure 6 allows us to say a few words on impulsively generated kink waves in coronal slabs, in which context streamer waves are likely to be relevant. Suppose that these waves result from the lateral impingement on a coronal slab by, say, a bulk of mass (coronal mass ejections in the case of streamer waves, see e.g., Chen *et al.* 2010, Feng *et al.* 2011, Decraemer, Zhukov, and Van Doorselaere 2020). It seems observationally difficult to tell the characteristics of the interaction

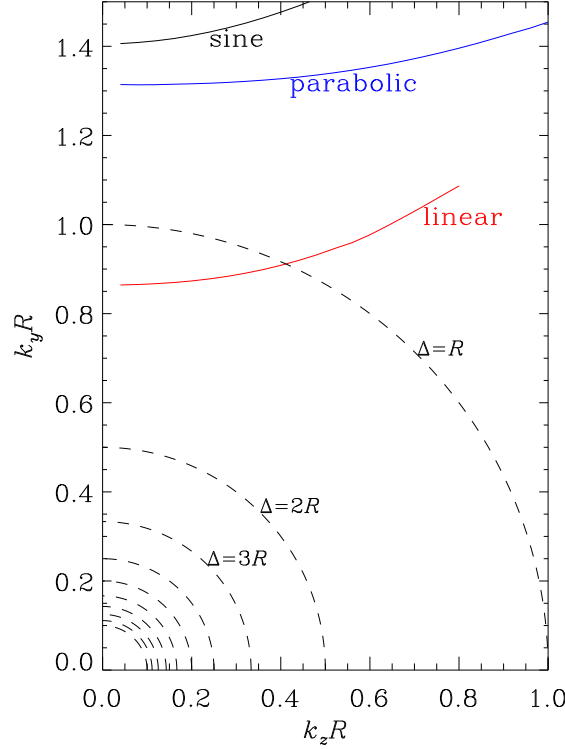


Figure 6. Influence of the density profile prescription on the dispersive properties of resonantly damped kink modes in coronal slabs. The solid curves in different colors pertain to the pair of $[k_y, k_z]$ where $|\omega_I/\omega_R|$ attains $1/2\pi$ at a fixed $l/R = 0.5$ for different density profiles as labeled. The density contrast is fixed at $\rho_i/\rho_e = 10$. Any dashed curve corresponds to those combinations of $[k_y, k_z]$ where the power spectral density drops from its maximum by a factor of e for some initial perturbation that depends on x and y as $\exp[-(x^2 + y^2)/2\Delta^2]$. A uniform spacing of R is adopted for Δ to plot the dashed curves, the outermost one pertaining to $\Delta = R$. See the text for details.

between the slab and, say, the mass motion. To make some quantitative progress, we nonetheless assume that the duration of the interaction is shorter than the (quasi-)periods of the resulting waves. We further assume that the interaction is spatially isotropic in the $x - y$ plane (see Figure 1a) and specifically possesses a Gaussian form $\exp[-(x^2 + y^2)/2\Delta^2]$. Evidently, Δ measures the spatial extent of the interaction. The power spectral density (PSD) is then $\propto \exp[-(k_y^2 + k_z^2)\Delta^2]$, and therefore decreases from its maximum by a factor of e along a circle of radius $1/\Delta$ in the $k_y - k_z$ plane. The dashed circles in Figure 6 correspond to a series of Δ uniformly spaced by R , with the outermost one corresponding to $\Delta = R$. Two situations then arise regarding the damping of the components constituting an impulsive wave. If $\Delta \gtrsim 2R$, then the majority of the components can survive resonant damping. If $\Delta \lesssim R$ instead, then the heavy resonant damping of the components pertaining to the upper left corner in Figure 6 will make it difficult for them to propagate to large distances. While these statements are enabled by Figure 6, this figure alone does not allow us to tell the eventual temporal and

spatial variations of impulsively generated waves. To name but one intricacy, we note that wave dispersion is well known to play a critical role in the dynamics of impulsive waves in both cylindrical (e.g., Roberts, Edwin, and Benz 1983; Edwin and Roberts 1986; Oliver, Ruderman, and Terradas 2014, 2015; Shestov, Nakariakov, and Kuzin 2015; Yu *et al.* 2016, 2017) and Cartesian equilibria (e.g., Edwin, Roberts, and Hughes 1986; Murawski and Roberts 1993; Nakariakov *et al.* 2004; Pascoe, Nakariakov, and Kupriyanova 2013; Yu, Nakariakov, and Yan 2016; Li *et al.* 2018; Goddard, Nakariakov, and Pascoe 2019). Of particular relevance is the one by Murawski and Roberts (1993), who performed two-dimensional (2D) time-dependent simulations to examine the response of a coronal slab to a lateral exciter. An extension of this study to 3D will clarify the behavior of the impulsively generated waves when the spatial extent of the driver is finite in the y -direction. Consequently, our eigenmode analysis involving a finite k_y will be much relevant, as we have practiced previously in other contexts (e.g., Yu *et al.* 2017; Li *et al.* 2018).

4. SUMMARY

This study was motivated by the apparent lack of an extensive survey of the parameters that may influence the resonant damping of kink modes in straight coronal slabs. To this end, we worked in the framework of pressure-less, gravity-free, resistive MHD and adopted an eigenvalue problem (EVP) approach. The equilibrium density was restricted to be structured only in the x -direction, but was allowed to take a rather generic form comprising a uniform interior, a uniform exterior, and a continuous transition layer (TL) in between. Inspired by examinations on resonantly damped kink modes in coronal cylinders (Soler *et al.* 2013, 2014), we paid special attention to the effects of the mathematical form for describing the density profile (“profile” for brevity). By doing this we generalized the study by Arregui *et al.* (2007a), who addressed an identical problem but nonetheless took a particular profile and examined only the influence of the out-of-plane wavenumber k_y . We additionally conducted an analytical study in the thin-boundary (TB) limit, and the resulting expressions generalized previous results by allowing a broader set of profile choices and/or a broader range of k_y .

Our results are summarized as follows. Technically speaking, we find that the eigenfrequencies computed with the self-consistent resistive approach tend to agree better with the analytical rather than the numerical solutions to the dispersion relation (20) derived in the TB limit. We therefore recommend expressions similar to Equations (21) and (22) for one to validate numerical studies on resonantly damped kink modes in an equilibrium similar to ours. Physically speaking, we find that the eigenfrequencies in general, and the damping efficiency in particular, are sensitive to how the density profile is formulated. In particular, the ratio of the imaginary to the real part of the eigenfrequency for the linear profile can readily exceed its sine counterpart by a factor of two or so. We also connected our computations to impulsively generated kink waves in coronal slabs by assuming that the impulsive driver depends on $x - y$ in a Gaussian form characterized by a spatial scale Δ . In the parameter range we examined, we find

that resonant absorption becomes relevant when $\Delta \lesssim R$, strongly damping those components with $k_y \gtrsim 1/R$ where R is the slab half-width.

Coronal structures are admittedly way more complicated than modeled here, in which context we name only two intricacies before closing. First, it proves observationally difficult to tell the mathematical form for the density profile, one primary culprit being that the corona is optically thin in, say, EUV. Seeing coronal loops as cylinders, one way to tackle this issue has been to experiment with a number of profiles and contrast the forward-modeled EUV intensities with measurements by, say, TRACE (e.g., Aschwanden *et al.* 2003) or SDO/AIA (e.g., Pascoe *et al.* 2017). However, while there is strong evidence that the density distribution is continuous rather than discontinuous, a statistical survey indicates that it is difficult to further discriminate between different profiles (Goddard *et al.* 2017). Second, structural curvature needs to be accounted for when oscillations in, say, active region arcades are examined. A step forward is to consider a cylindrical system (r, θ, y) and assume that the equilibrium magnetic field \mathbf{B}_0 is of the form $\hat{\theta}/r$. When $k_y \neq 0$, resonant absorption was shown to remain relevant by Hindman and Jain (2018), who nonetheless assumed a particular density profile to ensure that kink modes are trapped. For other profiles, however, lateral leakage is in general operational (e.g., Verwichte, Foullon, and Nakariakov 2006; Díaz, Zaqarashvili, and Roberts 2006), even though this effect tends to weaken with k_y (Rial *et al.* 2013, R13)³. We take these intricacies as strengthening rather than weakening the need for further examinations of coronal kink modes in a slab configuration. Regarding the first intricacy, that the eigenfrequencies are sensitive to profile choices can be employed in conjunction with the forward-modeling approach to tighten the constraints on the profile description, as has been practiced by Pascoe *et al.* (2018) who adopted a cylindrical geometry. Likewise, the second intricacy means that a systematic study is needed to assess the importance of resonant absorption relative to lateral leakage for kink modes in curved slabs, which has been initiated by R13. All these developments are warranted, but nonetheless are left for future studies.

Acknowledgments This research was supported by the National Natural Science Foundation of China (HY:41704165, BL: 41674172, 11761141002, 41974200; SXC:41604145), and by Shandong University via grant No 2017JQ07. We also acknowledge the International Space Science Institute-Beijing (ISSI-BJ) for supporting the international teams “MHD Seismology of the Solar Corona”, and “Pulsations in solar flares: matching observations and models”.

References

- Allcock, M., Erdélyi, R.: 2017, Magnetohydrodynamic Waves in an Asymmetric Magnetic Slab. *Sol. Phys.* **292**(2), 35. DOI. ADS. [2017SoPh...292...35A]

³Note that the equilibrium magnetic field adopted by R13 is somehow different from the one described by $\hat{\theta}/r$.

- Allian, F., Jain, R., Hindman, B.W.: 2019, A New Analysis Procedure for Detecting Periodicities within Complex Solar Coronal Arcades. *ApJ* **880**(1), 3. DOI. ADS. [2019ApJ...880...3A]
- Andries, J., Tirry, W.J., Goossens, M.: 2000, Modified Kelvin-Helmholtz Instabilities and Resonant Flow Instabilities in a One-dimensional Coronal Plume Model: Results for Plasma $\beta=0$. *ApJ* **531**(1), 561. DOI. ADS. [2000ApJ...531..561A]
- Anfinogentov, S.A., Nakariakov, V.M.: 2019, Magnetohydrodynamic Seismology of Quiet Solar Active Regions. *ApJ* **884**(2), L40. DOI. ADS. [2019ApJ...884L..40A]
- Arregui, I.: 2015, Wave heating of the solar atmosphere. *Philosophical Transactions of the Royal Society of London Series A* **373**(2042), 20140261. DOI. ADS. [2015RSPTA.37340261A]
- Arregui, I.: 2018, Bayesian coronal seismology. *Advances in Space Research* **61**(2), 655. DOI. ADS. [2018AdSpR...61..655A]
- Arregui, I., Asensio Ramos, A.: 2014, Determination of the cross-field density structuring in coronal waveguides using the damping of transverse waves. *A&A* **565**, A78. DOI. ADS. [2014A&A...565A..78A]
- Arregui, I., Goossens, M.: 2019, No unique solution to the seismological problem of standing kink magnetohydrodynamic waves. *A&A* **622**, A44. DOI. ADS. [2019A&A...622A..44A]
- Arregui, I., Terradas, J., Oliver, R., Ballester, J.L.: 2007a, Resonantly Damped Surface and Body MHD Waves in a Solar Coronal Slab with Oblique Propagation. *Sol. Phys.* **246**(1), 213. DOI. ADS. [2007SoPh...246..213A]
- Arregui, I., Terradas, J., Oliver, R., Ballester, J.L.: 2007b, The influence of the internal structuring of coronal loops on the properties of their damped transverse oscillations. *A&A* **466**(3), 1145. DOI. ADS. [2007A&A...466.1145A]
- Aschwanden, M.J., Nakariakov, V.M., Melnikov, V.F.: 2004, Magnetohydrodynamic Sausage-Mode Oscillations in Coronal Loops. *ApJ* **600**(1), 458. DOI. ADS. [2004ApJ...600..458A]
- Aschwanden, M.J., Fletcher, L., Schrijver, C.J., Alexander, D.: 1999, Coronal Loop Oscillations Observed with the Transition Region and Coronal Explorer. *ApJ* **520**(2), 880. DOI. ADS. [1999ApJ...520..880A]
- Aschwanden, M.J., Nightingale, R.W., Andries, J., Goossens, M., Van Doorsselaere, T.: 2003, Observational Tests of Damping by Resonant Absorption in Coronal Loop Oscillations. *ApJ* **598**(2), 1375. DOI. ADS. [2003ApJ...598.1375A]
- Ballester, J.L., Erdélyi, R., Hood, A.W., Leibacher, J.W., Nakariakov, V.M.: 2007, Preface: A Topical Issue in Honor of Professor Bernard Roberts. *Sol. Phys.* **246**(1), 1. DOI. ADS. [2007SoPh...246...1B]
- Cally, P.S.: 1986, Leaky and Non-Leaky Oscillations in Magnetic Flux Tubes. *Sol. Phys.* **103**(2), 277. DOI. ADS. [1986SoPh...103..277C]
- Chen, L., Hasegawa, A.: 1974, Plasma heating by spatial resonance of Alfvén wave. *Physics of Fluids* **17**(7), 1399. DOI. ADS. [1974PhF1...17.1399C]
- Chen, S.-X., Li, B., Shi, M., Yu, H.: 2018a, Damping of Slow Surface Sausage Modes in Photospheric Waveguides. *ApJ* **868**(1), 5. DOI. ADS. [2018ApJ...868...5C]
- Chen, S.-X., Li, B., Kumar, S., Yu, H., Shi, M.: 2018b, Fast Standing Modes in Transversely Nonuniform Solar Coronal Slabs: The Effects of a Finite Plasma Beta. *ApJ* **855**(1), 47. DOI. ADS. [2018ApJ...855...47C]
- Chen, S.-X., Li, B., Van Doorsselaere, T., Goossens, M., Yu, H., Geeraerts, M.: 2020, Damping of slow surface kink modes in solar photospheric waveguides modeled by one-dimensional inhomogeneities. *arXiv e-prints*, arXiv:2012.15426. ADS. [2020arXiv201215426C]
- Chen, Y., Song, H.Q., Li, B., Xia, L.D., Wu, Z., Fu, H., Li, X.: 2010, Streamer Waves Driven by Coronal Mass Ejections. *ApJ* **714**(1), 644. DOI. ADS. [2010ApJ...714..644C]
- Chen, Y., Feng, S.W., Li, B., Song, H.Q., Xia, L.D., Kong, X.L., Li, X.: 2011, A Coronal Seismological Study with Streamer Waves. *ApJ* **728**(2), 147. DOI. ADS. [2011ApJ...728..147C]
- Cranmer, S.R., Winebarger, A.R.: 2019, The Properties of the Solar Corona and Its Connection to the Solar Wind. *ARA&A* **57**, 157. DOI. ADS. [2019ARA&A...57..157C]
- De Moortel, I., Nakariakov, V.M.: 2012, Magnetohydrodynamic waves and coronal seismology: an overview of recent results. *Philosophical Transactions of the Royal Society of London Series A* **370**(1970), 3193. DOI. ADS. [2012RSPTA.370.3193D]
- Decraemer, B., Zhukov, A.N., Van Doorsselaere, T.: 2019, Three-dimensional Density Structure of a Solar Coronal Streamer Observed by SOHO/LASCO and STEREO/COR2 in Quadrature. *ApJ* **883**(2), 152. DOI. ADS. [2019ApJ...883..152D]
- Decraemer, B., Zhukov, A.N., Van Doorsselaere, T.: 2020, Properties of Streamer Wave Events Observed during the STEREO Era. *ApJ* **893**(1), 78. DOI. ADS. [2020ApJ...893...78D]

- Díaz, A.J., Zaqarashvili, T., Roberts, B.: 2006, Fast magnetohydrodynamic oscillations in a force-free line-tied coronal arcade. *A&A* **455**(2), 709. DOI. ADS. [2006A&A...455..709D]
- Edwin, P.M., Roberts, B.: 1982, Wave Propagation in a Magnetically Structured Atmosphere - Part Three - the Slab in a Magnetic Environment. *Sol. Phys.* **76**(2), 239. DOI. ADS. [1982SoPh...76..239E]
- Edwin, P.M., Roberts, B.: 1983, Wave Propagation in a Magnetic Cylinder. *Sol. Phys.* **88**(1-2), 179. DOI. ADS. [1983SoPh...88..179E]
- Edwin, P.M., Roberts, B.: 1986, Impulsively generated fast coronal pulsations. In: *NASA Conference Publication, NASA Conference Publication* **2449**, 347. ADS. [1986NASCP2449..347E]
- Edwin, P.M., Roberts, B.: 1988, Employing analogies for ducted MHD waves in dense coronal structures. *A&A* **192**(1-2), 343. ADS. [1988A&A...192..343E]
- Edwin, P.M., Roberts, B., Hughes, W.J.: 1986, Dispersive ducting of MHD waves in the plasma sheet: A source of Pi2 wave bursts. *Geophys. Res. Lett.* **13**(4), 373. DOI. ADS. [1986GeoRL...13..373E]
- Erdélyi, R., Goossens, M.: 2011, Magnetohydrodynamic Waves and Seismology of the Solar Atmosphere. *Space Sci. Rev.* **158**(2-4), 167. DOI. ADS. [2011SSRv...158..167E]
- Feng, S.W., Chen, Y., Li, B., Song, H.Q., Kong, X.L., Xia, L.D., Feng, X.S.: 2011, Streamer Wave Events Observed in Solar Cycle 23. *Sol. Phys.* **272**(1), 119. DOI. ADS. [2011SoPh...272..119F]
- Goddard, C.R., Nakariakov, V.M., Pascoe, D.J.: 2019, Fast magnetoacoustic wave trains with time-dependent drivers. *A&A* **624**, L4. DOI. ADS. [2019A&A...624L...4G]
- Goddard, C.R., Pascoe, D.J., Anfinogentov, S., Nakariakov, V.M.: 2017, A statistical study of the inferred transverse density profile of coronal loop threads observed with SDO/AIA. *A&A* **605**, A65. DOI. ADS. [2017A&A...605A..65G]
- Goossens, M., Andries, J., Aschwanden, M.J.: 2002, Coronal loop oscillations. An interpretation in terms of resonant absorption of quasi-mode kink oscillations. *A&A* **394**, L39. DOI. ADS. [2002A&A...394L...39G]
- Goossens, M., Erdélyi, R., Ruderman, M.S.: 2011, Resonant MHD Waves in the Solar Atmosphere. *Space Sci. Rev.* **158**(2-4), 289. DOI. ADS. [2011SSRv...158..289G]
- Goossens, M., Hollweg, J.V., Sakurai, T.: 1992, Resonant Behaviour of Magnetohydrodynamic Waves on Magnetic Flux Tubes - Part Three. *Sol. Phys.* **138**(2), 233. DOI. ADS. [1992SoPh...138..233G]
- Goossens, M., Arregui, I., Ballester, J.L., Wang, T.J.: 2008, Analytic approximate seismology of transversely oscillating coronal loops. *A&A* **484**(3), 851. DOI. ADS. [2008A&A...484..851G]
- Grossmann, W., Tataronis, J.: 1973, Decay of MHD waves by phase mixing. *Zeitschrift für Physik* **261**(3), 217. DOI. ADS. [1973ZPhy...261..217G]
- Guo, M.-Z., Chen, S.-X., Li, B., Xia, L.-D., Yu, H.: 2016, Inferring Flare Loop Parameters with Measurements of Standing Sausage Modes. *Sol. Phys.* **291**(3), 877. DOI. ADS. [2016SoPh...291..877G]
- Hasegawa, A., Chen, L.: 1974, Plasma Heating by Alfvén-Wave Phase Mixing. *Phys. Rev. Lett.* **32**(9), 454. DOI. ADS. [1974PhRvL...32..454H]
- Hindman, B.W., Jain, R.: 2018, A Novel Approach to Resonant Absorption of the Fast Magnetohydrodynamic Eigenmodes of a Coronal Arcade. *ApJ* **858**(1), 6. DOI. ADS. [2018ApJ...858....6H]
- Hollweg, J.V., Yang, G.: 1988, Resonance absorption of compressible magnetohydrodynamic waves at thin “surfaces”. *J. Geophys. Res.* **93**(A6), 5423. DOI. ADS. [1988JGR....93.5423H]
- Hornsey, C., Nakariakov, V.M., Fludra, A.: 2014, Sausage oscillations of coronal plasma slabs. *A&A* **567**, A24. DOI. ADS. [2014A&A...567A..24H]
- Ionson, J.A.: 1978, Resonant absorption of Alfvénic surface waves and the heating of solar coronal loops. *ApJ* **226**, 650. DOI. ADS. [1978ApJ...226..650I]
- Jain, R., Maurya, R.A., Hindman, B.W.: 2015, Fundamental-mode Oscillations of Two Coronal Loops within a Solar Magnetic Arcade. *ApJ* **804**(1), L19. DOI. ADS. [2015ApJ...804L..19J]
- Kwon, R.-Y., Ofman, L., Olmedo, O., Kramar, M., Davila, J.M., Thompson, B.J., Cho, K.-S.: 2013, STEREO Observations of Fast Magnetosonic Waves in the Extended Solar Corona Associated with EIT/EUV Waves. *ApJ* **766**(1), 55. DOI. ADS. [2013ApJ...766...55K]

- Li, B., Guo, M.-Z., Yu, H., Chen, S.-X.: 2018, Impulsively Generated Wave Trains in Coronal Structures. II. Effects of Transverse Structuring on Sausage Waves in Pressureless Slabs. *ApJ* **855**(1), 53. DOI. ADS. [2018ApJ...855...53L]
- Lopin, I., Nagorny, I.: 2015, Sausage Waves in Transversely Nonuniform Monolithic Coronal Tubes. *ApJ* **810**(2), 87. DOI. ADS. [2015ApJ...810...87L]
- Mok, Y., Einaudi, G.: 1985, Resistive decay of Alfvén waves in a non-uniform plasma. *Journal of Plasma Physics* **33**(2), 199. DOI. ADS. [1985JPlPh...33..199M]
- Murawski, K., Roberts, B.: 1993, Numerical Simulations of Fast Magnetohydrodynamic Waves in a Coronal Plasma - Part Two. *Sol. Phys.* **144**(1), 101. DOI. ADS. [1993SoPh...144..101M]
- Nakariakov, V.M., Erdélyi, R.: 2009, Foreword. *Space Sci. Rev.* **149**(1-4), 1. DOI. ADS. [2009SSRv...149....1N]
- Nakariakov, V.M., Kolotkov, D.Y.: 2020, Magnetohydrodynamic Waves in the Solar Corona. *ARA&A* **58**, 441. DOI. ADS. [2020ARA&A...58..441N]
- Nakariakov, V.M., Ofman, L.: 2001, Determination of the coronal magnetic field by coronal loop oscillations. *A&A* **372**, L53. DOI. ADS. [2001A&A...372L..53N]
- Nakariakov, V.M., Ofman, L., Deluca, E.E., Roberts, B., Davila, J.M.: 1999, TRACE observation of damped coronal loop oscillations: Implications for coronal heating. *Science* **285**, 862. DOI. ADS. [1999Sci...285..862N]
- Nakariakov, V.M., Arber, T.D., Ault, C.E., Katsiyannis, A.C., Williams, D.R., Keenan, F.P.: 2004, Time signatures of impulsively generated coronal fast wave trains. *MNRAS* **349**(2), 705. DOI. ADS. [2004MNRAS.349..705N]
- Nakariakov, V.M., Pilipenko, V., Heilig, B., Jelínek, P., Karlický, M., Klimushkin, D.Y., Kolotkov, D.Y., Lee, D.-H., Nisticò, G., Van Doorselaere, T., Verth, G., Zimovets, I.V.: 2016, Magnetohydrodynamic Oscillations in the Solar Corona and Earth's Magnetosphere: Towards Consolidated Understanding. *Space Sci. Rev.* **200**(1-4), 75. DOI. ADS. [2016SSRv...200...75N]
- Oliver, R., Ruderman, M.S., Terradas, J.: 2014, Propagation and Dispersion of Transverse Wave Trains in Magnetic Flux Tubes. *ApJ* **789**(1), 48. DOI. ADS. [2014ApJ...789...48O]
- Oliver, R., Ruderman, M.S., Terradas, J.: 2015, Propagation and Dispersion of Sausage Wave Trains in Magnetic Flux Tubes. *ApJ* **806**(1), 56. DOI. ADS. [2015ApJ...806...56O]
- Oxley, W., Zsámberger, N.K., Erdélyi, R.: 2020, Standing MHD Waves in a Magnetic Slab Embedded in an Asymmetric Magnetic Plasma Environment: Surface Waves. *ApJ* **898**(1), 19. DOI. ADS. [2020ApJ...898...19O]
- Pascoe, D.J., Nakariakov, V.M., Kupriyanova, E.G.: 2013, Fast magnetoacoustic wave trains in magnetic funnels of the solar corona. *A&A* **560**, A97. DOI. ADS. [2013A&A...560A..97P]
- Pascoe, D.J., Goddard, C.R., Anfinogentov, S., Nakariakov, V.M.: 2017, Coronal loop density profile estimated by forward modelling of EUV intensity. *A&A* **600**, L7. DOI. ADS. [2017A&A...600L...7P]
- Pascoe, D.J., Anfinogentov, S.A., Goddard, C.R., Nakariakov, V.M.: 2018, Spatiotemporal Analysis of Coronal Loops Using Seismology of Damped Kink Oscillations and Forward Modeling of EUV Intensity Profiles. *ApJ* **860**(1), 31. DOI. ADS. [2018ApJ...860...31P]
- Poedts, S., Kerner, W.: 1991, Ideal quasimodes reviewed in resistive magnetohydrodynamics. *Phys. Rev. Lett.* **66**(22), 2871. DOI. ADS. [1991PhRvL...66.2871P]
- Rial, S., Arregui, I., Terradas, J., Oliver, R., Ballester, J.L.: 2013, Wave Leakage and Resonant Absorption in a Loop Embedded in a Coronal Arcade. *ApJ* **763**(1), 16. DOI. ADS. [2013ApJ...763...16R]
- Roberts, B.: 2019, *Mhd waves in the solar atmosphere*, Cambridge University Press, ??? DOI. [2019CUP_Roberts]
- Roberts, B., Edwin, P.M., Benz, A.O.: 1983, Fast pulsations in the solar corona. *Nature* **305**(5936), 688. DOI. ADS. [1983Natur.305..688R]
- Rosenberg, H.: 1970, Evidence for MHD Pulsations in the Solar Corona. *A&A* **9**, 159. ADS. [1970A&A....9..159R]
- Ruderman, M.S., Roberts, B.: 2002, The Damping of Coronal Loop Oscillations. *ApJ* **577**(1), 475. DOI. ADS. [2002ApJ...577..475R]
- Ruderman, M.S., Tirry, W., Goossens, M.: 1995, Non-stationary resonant Alfvén surface waves in one-dimensional magnetic plasmas. *Journal of Plasma Physics* **54**(2), 129. DOI. ADS. [1995JPlPh...54..129R]
- Sakurai, T., Goossens, M., Hollweg, J.V.: 1991, Resonant Behaviour of Magnetohydrodynamic Waves on Magnetic Flux Tubes - Part One. *Sol. Phys.* **133**(2), 227. DOI. ADS. [1991SoPh...133..227S]

- Sewell, G.: 1988, *The Numerical Solution of Ordinary and Partial Differential Equations*, San Diego: Academic Press, ????. [1988Sewell_PDE2D]
- Shestov, S., Nakariakov, V.M., Kuzin, S.: 2015, Fast Magnetoacoustic Wave Trains of Sausage Symmetry in Cylindrical Waveguides of the Solar Corona. *ApJ* **814**(2), 135. DOI. ADS. [2015ApJ...814..135S]
- Soler, R., Oliver, R., Ballester, J.L., Goossens, M.: 2009, Damping of Filament Thread Oscillations: Effect of the Slow Continuum. *ApJ* **695**(2), L166. DOI. ADS. [2009ApJ...695L.166S]
- Soler, R., Goossens, M., Terradas, J., Oliver, R.: 2013, The Behavior of Transverse Waves in Nonuniform Solar Flux Tubes. I. Comparison of Ideal and Resistive Results. *ApJ* **777**(2), 158. DOI. ADS. [2013ApJ...777..158S]
- Soler, R., Goossens, M., Terradas, J., Oliver, R.: 2014, The Behavior of Transverse Waves in Nonuniform Solar Flux Tubes. II. Implications for Coronal Loop Seismology. *ApJ* **781**(2), 111. DOI. ADS. [2014ApJ...781..111S]
- Spruit, H.C.: 1982, Propagation Speeds and Acoustic Damping of Waves in Magnetic Flux Tubes. *Sol. Phys.* **75**(1-2), 3. DOI. ADS. [1982SoPh...75....3S]
- Tataronis, J., Grossmann, W.: 1973, Decay of MHD waves by phase mixing. *Zeitschrift für Physik* **261**(3), 203. DOI. ADS. [1973ZPhy...261..203T]
- Tatsuno, T., Wakatani, M.: 1998, Damping of Surface Alfvén Wave in a Slab Plasma. *Journal of the Physical Society of Japan* **67**(7), 2322. DOI. ADS. [1998JPSJ...67.2322T]
- Terradas, J., Oliver, R., Ballester, J.L.: 2006, Damped Coronal Loop Oscillations: Time-dependent Results. *ApJ* **642**(1), 533. DOI. ADS. [2006ApJ...642..533T]
- Tirry, W.J., Goossens, M.: 1996, Quasi-Modes as Dissipative Magnetohydrodynamic Eigenmodes: Results for One-dimensional Equilibrium States. *ApJ* **471**, 501. DOI. ADS. [1996ApJ...471..501T]
- Van Doorsselaere, T., Andries, J., Poedts, S., Goossens, M.: 2004, Damping of Coronal Loop Oscillations: Calculation of Resonantly Damped Kink Oscillations of One-dimensional Nonuniform Loops. *ApJ* **606**(2), 1223. DOI. ADS. [2004ApJ...606.1223V]
- Van Doorsselaere, T., Nakariakov, V.M., Li, B., Antolin, P.: 2020, Editorial: Magnetohydrodynamic Waves in the Solar Atmosphere: Heating and Seismology. *Frontiers in Astronomy and Space Sciences* **6**, 79. DOI. ADS. [2020FrASS...6...79V]
- Verwichte, E., Foullon, C., Nakariakov, V.M.: 2006, Fast magnetoacoustic waves in curved coronal loops. *A&A* **446**(3), 1139. DOI. ADS. [2006A&A...446.1139V]
- Verwichte, E., Nakariakov, V.M., Cooper, F.C.: 2005, Transverse waves in a post-flare supracarade. *A&A* **430**, L65. DOI. ADS. [2005A&A...430L..65V]
- Wentzel, D.G.: 1979a, Hydromagnetic surface waves. *ApJ* **227**, 319. DOI. ADS. [1979ApJ...227..319W]
- Wentzel, D.G.: 1979b, The dissipation of hydromagnetic surface waves. *ApJ* **233**, 756. DOI. ADS. [1979ApJ...233..756W]
- Yang, Z., Bethge, C., Tian, H., Tomczyk, S., Morton, R., Del Zanna, G., McIntosh, S.W., Karak, B.B., Gibson, S., Samanta, T., He, J., Chen, Y., Wang, L.: 2020, Global maps of the magnetic field in the solar corona. *Science* **369**(6504), 694. DOI. ADS. [2020Sci...369..694Y]
- Yu, H., Li, B., Chen, S.-X., Guo, M.-Z.: 2015, Kink and Sausage Modes in Nonuniform Magnetic Slabs with Continuous Transverse Density Distributions. *ApJ* **814**(1), 60. DOI. ADS. [2015ApJ...814...60Y]
- Yu, H., Li, B., Chen, S.-X., Xiong, M., Guo, M.-Z.: 2016, Impulsively Generated Sausage Waves in Coronal Tubes with Transversally Continuous Structuring. *ApJ* **833**(1), 51. DOI. ADS. [2016ApJ...833...51Y]
- Yu, H., Li, B., Chen, S.-X., Xiong, M., Guo, M.-Z.: 2017, Impulsively Generated Wave Trains in Coronal Structures. I. Effects of Transverse Structuring on Sausage Waves in Pressureless Tubes. *ApJ* **836**(1), 1. DOI. ADS. [2017ApJ...836....1Y]
- Yu, S., Nakariakov, V.M., Yan, Y.: 2016, Effect of a Sausage Oscillation on Radio Zebra-pattern Structures in a Solar Flare. *ApJ* **826**(1), 78. DOI. ADS. [2016ApJ...826...78Y]
- Zajtsev, V.V., Stepanov, A.V.: 1975, On the origin of pulsations of type IV solar radio emission. Plasma cylinder oscillations (I). *Issledovaniia Geomagnetizmu Aeronomii i Fizike Solntsa* **37**, 3. ADS. [1975IGAFS...37....3Z]